



Relationship between the South Asian High and Western North Pacific tropical cyclone genesis

Yuqi Zang ^a, Haikun Zhao ^{a,*}, Philip J. Klotzbach ^b, Chao Wang ^a, Jian Cao ^a

^a Key Laboratory of Meteorological Disaster, Ministry of Education, Joint International Research Laboratory of Climate and Environment Change, Collaborative Innovation Center on Forecast and Evaluation of Meteorological Disaster, Nanjing University of Information Science and Technology, Nanjing, China

^b Department of Atmospheric Science, Colorado State University, Fort Collins, CO, USA

ARTICLE INFO

Keywords:

South Asian high
Tropical cyclone
Western North Pacific

ABSTRACT

This study highlights a significant inter-decadal modulation of the South Asian high (SAH) on the meridional distribution of western North Pacific (WNP) tropical cyclone genesis frequency (TCGF). There is an obvious inter-decadal change in the first leading SAH mode, with an abrupt weakening since the early 1990s. During 1979–1993, when there was a stronger SAH, TCs were suppressed over the northern WNP and enhanced over the southern WNP in response to inter-annual SAH changes. The northern WNP TCGF had a significant negative correlation with the SAH ($r = -0.69$), while the southern WNP TCGF had a significant positive correlation with the SAH ($r = 0.78$). This north-south seesaw pattern driven by the SAH weakened during 1994–2019.

This inter-decadal modulation of the inter-annual SAH-WNP TC genesis relationship can be explained by changes in large-scale environmental parameters. There is anomalous ascending (descending) motion and negative (positive) vorticity centered at 850-hPa as well as less (more) moisture at 600-hPa in the northern WNP (southern WNP) during 1979–1993. The maintenance of a strong low-level anomalous anticyclone accompanied by the concurrent influence of the SAH and East Asian upper-tropospheric jet stream decreases northern WNP TCGF. Linking to an El Niño-like SST pattern, the cyclonic circulation forced by a Gill-type forcing and enhanced by equatorial low-level westerly anomalies increases southern WNP TCGF. In contrast, we find a relatively weak inter-annual relationship of large-scale factors to the SAH since 1994. This weakening relationship is largely due to the inter-decadal weakening of the SAH and East Asian upper-tropospheric jet stream. Inter-decadal changes of the East Asian summer monsoon and the phase shift of the Atlantic Multi-decadal Oscillation appear to be two important factors modulating the inter-annual relationship between the SAH and the meridional distribution of WNP TCGF.

1. Introduction

On average, over the western North Pacific (WNP), there are ~ 27 tropical cyclones (TCs) per year, accounting for almost one-third of the world's annual TCs (Schreck III et al., 2014; Chan, 2005). Given the tremendous damage that TCs cause as well as uncertainty as to how TCs may change in a warming climate (Zhang et al., 2009; Peduzzi et al., 2012; Lu et al., 2021), a comprehensive understanding of the multi-scale variability of TCs is critical for both prediction as well as mitigation.

On inter-annual time scales, sea surface temperatures (SSTs) in various ocean basins can impact WNP TCs (Wang and Chan, 2002; Zhao et al., 2011, 2020; Zhan et al., 2011; Huo et al., 2015; Cao et al., 2016;

Yu et al., 2016; Zhang et al., 2016). El Niño-Southern Oscillation (ENSO) is generally considered to be one of the most important factors modulating WNP TC activity (Wang et al., 2000; Wang and Chan, 2002; Camargo and Sobel, 2005; Patricola et al., 2018; Zhao and Wang, 2016, 2019; Guo and Tan, 2018, 2021). ENSO has been shown to significantly modulate where WNP TCs preferentially form and subsequently track as well as the position of TC rapid intensification. These shifts in genesis and track lead to changes in TC intensity as well via changes in the large-scale atmospheric and oceanic environment. Most studies have found no significant relationship between ENSO and WNP TC frequency, however. Several studies have found that SST anomalies in both the East Indian Ocean via Kelvin wave propagation and the North Atlantic Ocean

* Corresponding author at: Pacific Typhoon Research Center, Key Laboratory of Meteorological Disaster of Ministry of Education, Nanjing University of Information Science and Technology, Nanjing, China.

E-mail address: haikunzhao@nuist.edu.cn (H. Zhao).

via a Gill-type response can significantly impact WNP TCs (Gill, 1980; Zhan et al., 2011; Ha et al., 2015; Huo et al., 2015; Cao et al., 2016; Yu et al., 2016). Other studies have highlighted the impact of trans-basin interactions among Indo-Pacific-Atlantic SST anomalies (SSTAs) on TC activity over various basins (Wang and Wang, 2019; Chen et al., 2021a; Chen et al., 2021b).

Given that large-scale circulation systems have relatively high predictability (Ritchie and Holland, 1999; Wang et al., 2013; Wang and Wu, 2018; Wang et al., 2019), more studies in recent years have focused on understanding TC variability via changes in the large-scale circulation instead of changes in large-scale parameters (Zhao and Raga, 2014; Liu et al., 2022; Wu et al., 2022). In the WNP, four large-scale circulation systems including the tropical upper-tropospheric trough, the South Asian high (SAH), the low-level monsoon trough and the West Pacific subtropical high (WPSH) were found to be the main large-scale circulation systems affecting TCs (Briegel and Frank, 1997; Wu et al., 2015; Wang and Wang, 2019, 2021; Wu et al., 2022). The mutual configuration of these large-scale circulation systems can largely determine TC genesis frequency (TCGF) location on inter-annual and inter-decadal time scales (Wu et al., 2012; Wang and Wu, 2016; Zhao and Wang, 2019). Studies have suggested that ~70% of WNP TCs were associated with the monsoon trough given its strong low-level convergence (Briegel and Frank, 1997; Ritchie and Holland, 1999; Chen et al., 2004). The tropical upper-tropospheric trough causes strong westerly vertical wind shear and can significantly decrease TCs over its southern flank, as well as exerting a significant impact on longitudinal shifts in TC genesis (Wu et al., 2015; Wang and Wu, 2016). Changes in the West Pacific subtropical high can be driven by trans-basin SST anomalies. These West Pacific subtropical high changes can modulate the WNP monsoon circulation and its oceanic environment, consequently modulating WNP TC activity (Liu and Chan, 2013; Wang et al., 2013; Wang and Wang, 2019). However, the impact of the SAH on WNP TCs has been relatively less studied.

The SAH is regarded to be one of the most important large-scale features in the upper troposphere during the boreal summer, with a semi-permanent anti-cyclonic circulation covering the entire South Asian continent (Mason and Anderson, 1963; Tao and Zhu, 1964; Krishnamurti et al., 1973). Its development and maintenance come from sensible heating over the Tibetan-Iran Plateau, which is usually associated with changes of the western North Pacific subtropical high (Flohn, 1957; Tao and Zhu, 1964; Hoskins and Rodwell, 1995). Several prior studies have suggested that the SAH can significantly affect Asian weather and climate (Peiquan et al., 2005; Liu et al., 2013; Ren et al., 2015; Shi and Qian, 2016; Yang and Li, 2016). More recently, Wang and Wang (2021) showed that the SAH and South China Sea TCGF during July–September are significantly negatively correlated during 1979–2017. The coupled effect between the SAH, the western North Pacific subtropical high and WNP TCGF was also investigated in other studies (Jiang et al., 2011; Ning et al., 2017). Although these studies have emphasized the possible importance of the SAH on WNP TCs, the impact of the SAH on WNP TCGF remains unclear.

This manuscript explores the inter-annual and inter-decadal relationship between WNP TCGF and the SAH. We hypothesize that changes in climate regimes may be occurring, given the long-term decreasing trend in SAH strength (Xue et al., 2015, 2017, 2018; Geng et al., 2020; Zhang et al., 2021). We investigate how this decreasing trend in SAH strength may modulate the relationship between the SAH and WNP TCGF. The remainder of the manuscript is organized as follows. Section 2 describes the data and methodology. Section 3 examines the inter-annual and inter-decadal relationship between the SAH and the meridional distribution of WNP TCGF. Section 4 explores the possible mechanisms. Section 5 summarizes the main results of this study.

2. Data and methodology

TC data from 1979 to 2020 are obtained from the Joint Typhoon

Warning Center (JTWC) best track dataset (Chu et al., 2002). This dataset includes information on TC location and maximum sustained wind at 6-h intervals. TCs with an intensity reaching or exceeding 34 kt (~17.2 m s⁻¹) (e.g., named storms) are considered in this study.

Monthly atmospheric fields are obtained from the National Centers for Environmental Prediction and National Center for Atmospheric Research (NCEP/NCAR) monthly Reanalysis II dataset with a 2.5° × 2.5° horizontal resolution and 17 vertical pressure levels (Kanamitsu et al., 2002). We also compare the magnitude of the SAH obtained from NCEP/NCAR Reanalysis II with results calculated from the ECMWF 5th (ERA5) reanalysis (Hersbach et al., 2020) and the Japanese 55-year (JRA-55) reanalysis (Kobayashi et al., 2015). Monthly SST are obtained from the National Oceanic and Atmospheric Administration (NOAA) Extended Reconstruction SST version 5 (ERSST v5) with a horizontal resolution of 2° × 2° (Huang et al., 2017). Monthly outgoing longwave radiation (OLR) data from NOAA (Liebmann and Smith, 1996) and monthly precipitation data from the Global Precipitation Climatology Project (Adler et al., 2018) are also used in this study. The monthly Atlantic multi-decadal oscillation (AMO) and Niño 3.4 index are obtained from the NCAR climate data guide (CDG) (Trenberth and National Center for Atmospheric Research Staff, 2020; Trenberth et al., 2021) (<https://climatedataguide.ucar.edu/climate-data>).

This study focuses on the peak TC season from July to September (JAS), accounting for ~55% of the annual total number of TCs in the WNP basin (0°–30°N, 120°E–180°E), excluding the South China Sea. To understand the association between the meridional dipole pattern of WNP TCGF and the SAH, the WNP basin is divided into two sub-regions: the northern WNP (NWNP: 17.5°N–30°N) and the southern WNP (SWNP: 0–17.5°N). We selected 17.5°N as the latitudinal dividing line mainly based on the observed TCGF seesaw pattern characterized by more TCs to the south and fewer TCs to the north when the SAH is stronger (Fig. 3a). To reduce the effect of increasing sea level pressure due to global warming (Wu and Wang, 2015; Wu et al., 2017), the leading mode of the SAH is obtained by multivariate empirical orthogonal function analysis of 200-hPa U and V following prior studies (Wang, 1992; Wang and Wang, 2021). Composite analysis, regression analysis, and correlation analysis were performed to explore the relationship between WNP TCGF and the SAH. Statistical significance is calculated at the 90% confidence level using a two-tailed Student's *t*-test unless specifically stated. Given the high autocorrelation of several of the variables investigated, the significance of correlations between two time series are investigated using effective degrees of freedom (Bretherton et al., 1999). A climate regime shift for the first leading mode of the SAH is identified using an 11-year moving *t*-test (MTT) (Xiao and Li, 2007; Xiao et al., 2012).

In this study, we adopt the dynamic genesis potential index (DGPI; Wang and Murakami, 2020) to examine the effect of large-scale dynamical environmental conditions on TC formation and to diagnose the relative importance of each term for WNP TCGF. The DGPI shows a better representation of inter-annual variability of TCs, especially over the WNP basin, than the widely-used genesis potential index proposed by Emanuel and Nolan (2004) (Murakami and Wang, 2022). The DGPI is defined as:

$$\text{DGPI} = (2 + 0.1V_s)^{-1.7} \left(5.5 - \frac{\partial u}{\partial y} 10^5 \right)^{2.3} (5 - 20\omega)^{3.3} (5.5 + |10^5 \eta|)^{2.4} e^{-11.8} - 1$$

where V_s is the magnitude of vertical wind shear (VWS) between 200 and 850-hPa, $\partial u / \partial y$ is the meridional gradient of zonal wind at 500-hPa, ω is 500-hPa vertical velocity, and η is 850-hPa absolute vorticity.

3. Recent changes in SAH-WNP TC relationship

3.1. Inter-decadal changes in the SAH leading mode

Fig. 1a shows the first leading EOF mode of 200-hPa winds over the

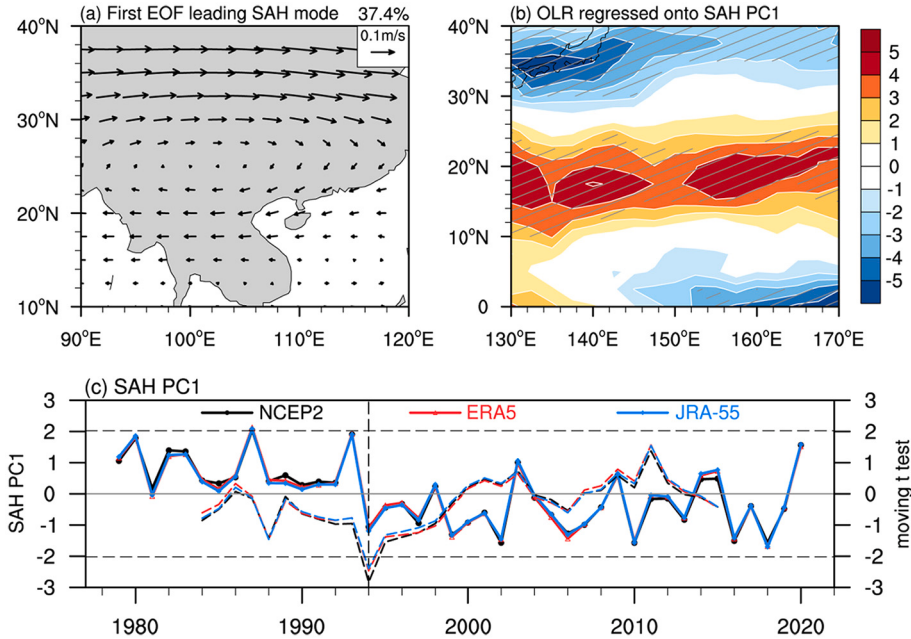


Fig. 1. (a) First leading mode obtained by multivariate EOF analysis of mean 200 hPa wind (vectors, m s^{-1}) over 10°N - 40°N , 90°E - 140°E during July–September of 1979–2020. (b) Regressed outgoing long-wave radiation (OLR) anomalies (shaded, W m^{-2}) against PC1 of the SAH during 1979–2020. Only regressions significant at the 90% confidence level are displayed. (c) Standardized time series of principal components (PC1) of the first leading SAH mode from NCEP2, ERA5 and JRA-55 reanalysis datasets, and an 11-year moving *t*-test for PC1 from the three reanalysis datasets.

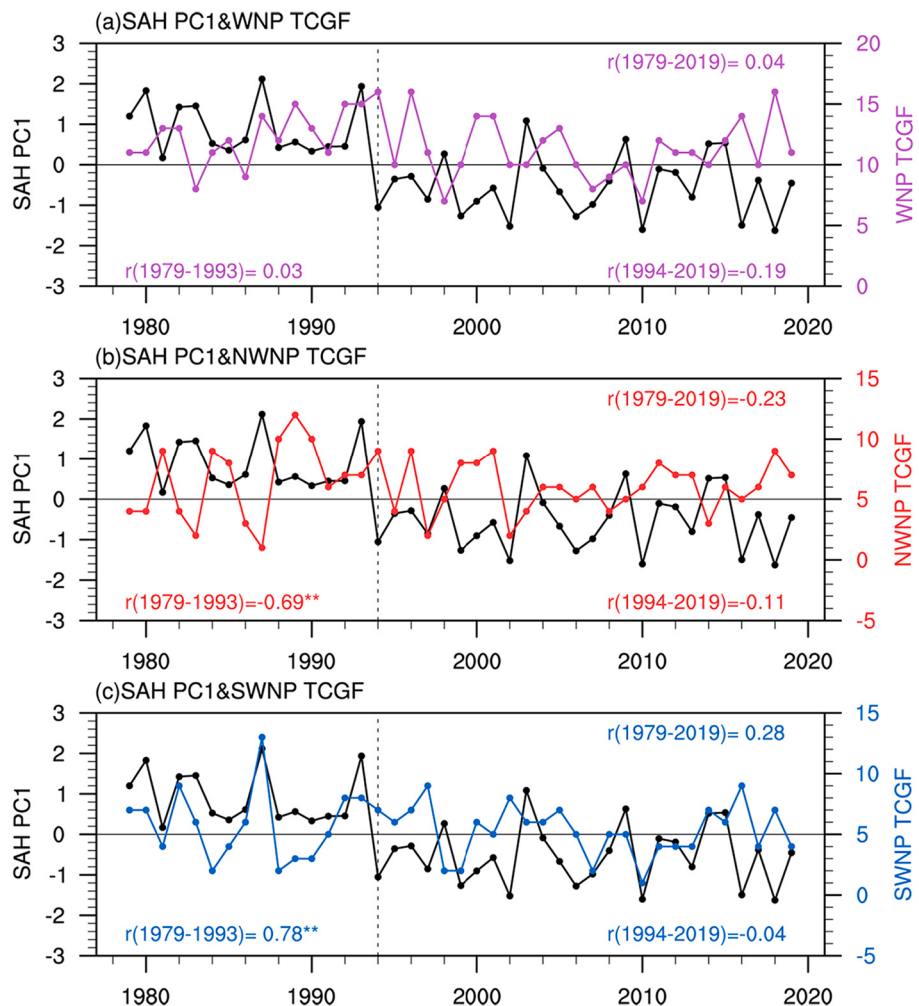


Fig. 2. Time series of PC1 and TCGF (a) over the WNP basin excluding the South China Sea [0 – 30°N , 120 – 180°E], (b) the northern WNP (NWNP) region [0 – 17.5°N , 120°E – 180°E] and (c) the southern WNP (SWNP) region [17.5°N – 30°N , 120°E – 180°E]. Correlations (*r*) during the whole period of 1979–2019 and the two sub-periods of 1979–1993 and 1994–2019 are shown, with “**” indicating values that are significant at a 90% confidence level.

SAH region (10°N - 40°N , 90°E - 120°E). This mode explains 37% of the total variance and is characterized by an anomalously strong anticyclonic circulation over the northern part of the Indochina Peninsula. Previous studies have shown that the SAH exhibits a bimodal distribution between the Tibetan mode and the Iranian mode due to east-west shifts in its center (Zhang et al., 2002; Zhou et al., 2009; Niitze et al., 2016). The first leading mode shown in Fig. 1a reflects the Tibetan mode given its intensity distribution. When OLR anomalies are regressed onto the first SAH leading mode principal component (PC1) during 1979–2020 as shown in Fig. 1b, we find a positive area over the WNP main development region during the peak TC season likely modulating WNP TCs. It agrees with prior studies on the suppressed convection over the WNP basin in response to the stronger SAH (Zhao et al., 2009; Jiang et al., 2011; Wei et al., 2019).

Consistent with prior studies (Zhang et al., 2021), we find an obvious inter-decadal change in the SAH (Fig. 1c), with decreasing SAH intensity from 1994 to 2019. In 2020, however, the SAH is stronger. The moving t-test method further confirms the abrupt change point of 1994. We find a similar change point in the first leading SAH mode using the ERA5 or JRA-55 reanalysis as we do using NCEP2 reanalysis data, indicating that the change point is not reanalysis dependent. Given the robustness of inter-decadal changes of the first SAH leading mode, we focus on the two sub-periods of 1979–1993 and 1994–2019 in this study.

3.2. Recent weakening of the SAH modulation of the meridional distribution of TCGF

During the full period from 1979 to 2019, there is no significant association between WNP TCGF and the SAH first leading mode (Fig. 2). PC1 has a similar insignificant correlation with both SWNP TCGF ($r = 0.28$) and NWNP TCGF ($r = -0.23$). Additionally, we compute the inter-annual relationship between TCGF and PC1 for the two sub-periods and found no significant correlation (Fig. 2a). However, the inter-annual relationship between the meridional distribution of TCGF and PC1 shows an apparent climate regime shift. During 1979–1993, there is a significant negative ($r = -0.69$) inter-annual correlation between PC1 and NWNP TCGF. In contrast, there is a significant positive correlation ($r = 0.78$) between PC1 and SWNP TCGF (Fig. 2b, c). However, this close association between the meridional distribution of WNP TCs and the SAH does not occur during the more recent sub-period from 1994 to 2019 (Fig. 2b, c). In summary, the SAH-driven north-south dipole pattern of WNP TCGF was present from 1979 to 1993 but has weakened from 1994 to 2019.

To further understand the meridional dipole pattern of TC distribution over the WNP basin in response to inter-annual changes in the SAH for different inter-decadal sub-periods, we select the five strongest and five weakest SAH years based on the normalized PC1 for the two sub-periods. We then perform composite analysis (Fig. 3). At first glance, there is an obvious north-south seesaw pattern during 1979–1993, while this see-saw pattern is relatively weak during 1994–2019. During 1979–1993, 43 TCs formed over the SWNP region, and 18 TCs formed over the NWNP region during strong SAH years. The opposite case can be found for weak SAH years during the period of 1979–1993, with more TCs over the NWNP (40 TCs) and fewer TCs over the SWNP (24 TCs). The difference in TCs between the SWNP and NWNP regions are significant for both strong SAH and weak SAH years. However, as shown in Fig. 3b, the latitudinal difference in TCs between the NWNP and the SWNP regions for strong SAH and weak SAH years during the period of 1994–2019 becomes weak and insignificant.

3.3. Recent changes in the large-scale environment associated with inter-annual SAH variability

To understand a climate regime shift in the inter-annual association between the meridional distribution of TCs over the WNP basin and the SAH, corresponding inter-decadal changes in the large-scale

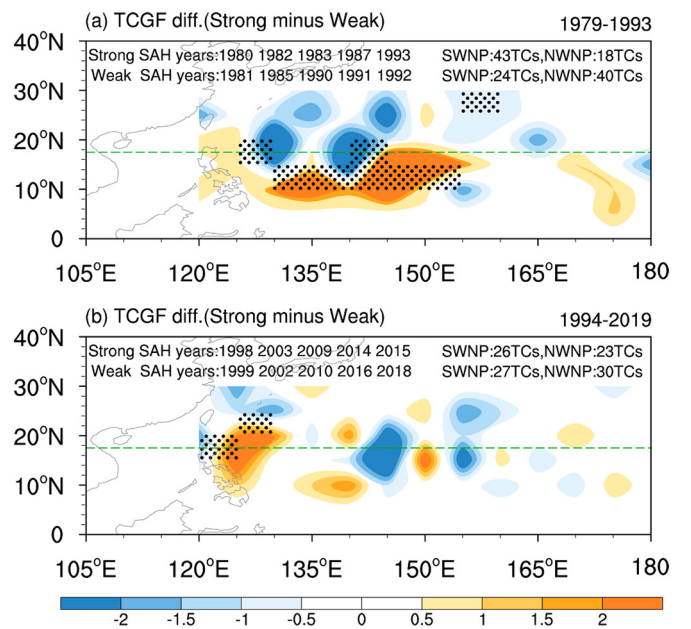


Fig. 3. Composite July–September TCGF distribution difference for the period of (a) 1979–1993 and (b) 1994–2019 in the WNP basin (0 – 30°N , 120°E – 180°E) between strong and weak SAH years. The years selected and the total number of TCs for each composite set are also displayed. The values in (a) and (b) with black dots are significant at the 90% confidence level.

environment are examined in this section. Vertical wind shear, low-level vorticity, mid-level vertical velocity and mid-level moisture are regressed onto PC1 for both sub-periods (Fig. 4). There is a north-south seesaw regression pattern for all four large-scale factors during 1979–1993, favoring the SAH-driven meridional dipole pattern of TCs over the WNP basin (Fig. 4a-d). In contrast, these north-south seesaw regression patterns still exist from 1994 to 2019 but become relatively weak (Fig. 4e-h), likely causing the weakening of the inter-annual relationship between the SAH and the meridional distribution of WNP TCs.

The DGPI is adopted to further confirm the importance of large-scale factors in response to the SAH. As shown in Fig. 5, DGPI regressions onto PC1 show a clear north-south seesaw pattern during 1979–1993 but become relatively weak during 1994–2019, consistent with the TCGF regression onto PC1 shown in Fig. 2. We next examine the role of large-scale factors in the climate regime shift of the meridional dipole pattern based upon a budget analysis of the DGPI (Fig. 5c-d). During 1979–1993, the main DGPI contributors to the TC modulation over the NWNP basin come from the meridional gradient of the zonal wind at 500-hPa and 500-hPa vertical velocity, while the main contributors for TCs over the SWNP are the meridional gradient of zonal wind at 500-hPa and 850-hPa absolute vorticity (Fig. 5c). These results indicate that the factors affecting TCs in the SWNP and NWNP are different, with vertical motion dominating the NWNP and the low- and mid-level circulation dominating the SWNP. Additionally, vertical wind shear in the WNP plays a role in TC formation for both sub-regions (Fig. 5c-d). During 1994–2019, the out-of-phase DGPI relationship in the NWNP and SWNP disappear; with anomalies reduced for both sub-regions but especially for the NWNP (Fig. 5d). The reduction of changes in 500-hPa vertical velocity likely play the largest role in reducing DGPI over the WNP basin.

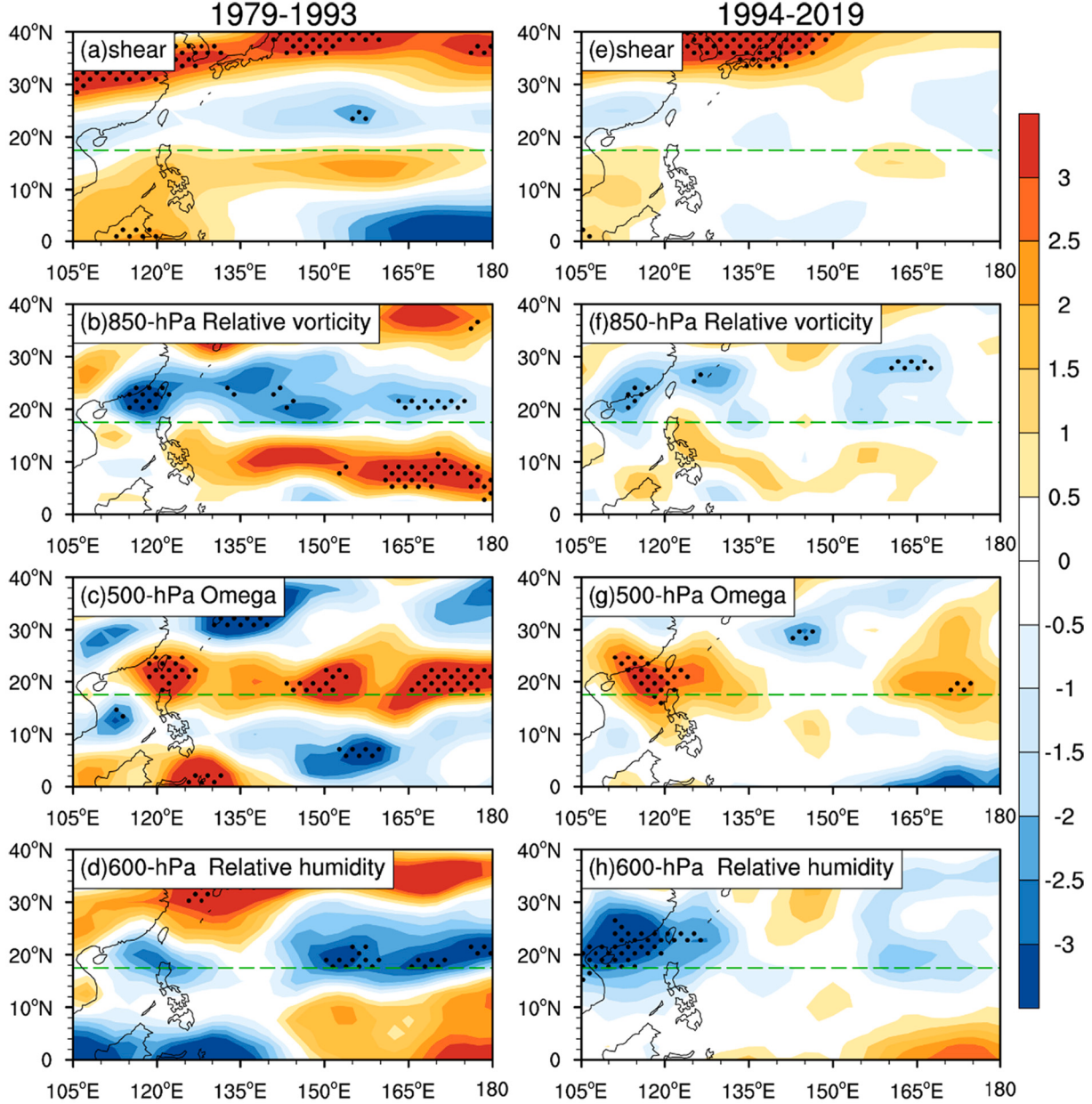


Fig. 4. Regressed (a, e) vertical wind shear (shading, units: m s^{-1}), (b, f) 850-hPa relative vorticity (shading, units: 10^{-6} s^{-1}), (c, g) 500-hPa vertical velocity (shading, 3×10^{-2} units: Pa s^{-1}), and (d, h) 600-hPa relative humidity (shading, units: %) against SAH PC1 during July–September from 1979 to 1993 (left panels) and 1994–2019 (right panels). The values with dots are significant at the 90% confidence level. The 17.5°N latitude line used as the boundary between the NWNP and SWNP regions is highlighted with a green dashed line. (For interpretation of the references to colour in this figure legend, the reader is referred to the web version of this article.)

4. Physical discussion

4.1. Role of the climate regime shift in the inter-annual SAH-WNP TCGF relationship

How does the SAH at 200-hPa affect the large-scale low- and mid-level circulation over the WNP basin? Fig. 6 shows regressed patterns of winds, relative vorticity and height onto SAH PC1 for both sub-periods. During 1979–1993, the SAH appears stronger and tends to move southward. The strong negative vorticity in the SAH can reach lower levels via descending motion (Fig. 6a, c) (Wei et al., 2019), resulting in an anomalous low-level anticyclone over the NWNP region (Fig. 6b). However, the negative vorticity transport from the SAH is not enough to affect the whole WNP as shown in Fig. 6b and c. Other large-

scale circulation systems likely contribute to this anomalous anticyclone over the NWNP region. During 1979–1993, the East Asian upper-tropospheric jet stream (EAJS), that is located in the northern part of the SAH, tends to move southward and intensify (Kwon, 2005), which would also concurrently enhance the upper-level subtropical North Pacific anomalous anticyclone (15°N – 35°N , 140°E – 170°W). The region is located south of the EAJS and would be influenced by anticyclonic shear, thus ultimately suppressing NWNP TCGF (Fig. 6a, b, c). In contrast, both the SAH and the EAJS become relatively weak in 1994–2019 compared to 1979–1993, weakening negative vorticity conveyance to the NWNP sub-region (Fig. 6e, g). This also results in a weaker anticyclone (Fig. 6f), leading to only a weak modulation of TCGF over the NWNP.

We next investigate changes in the large-scale environment over the

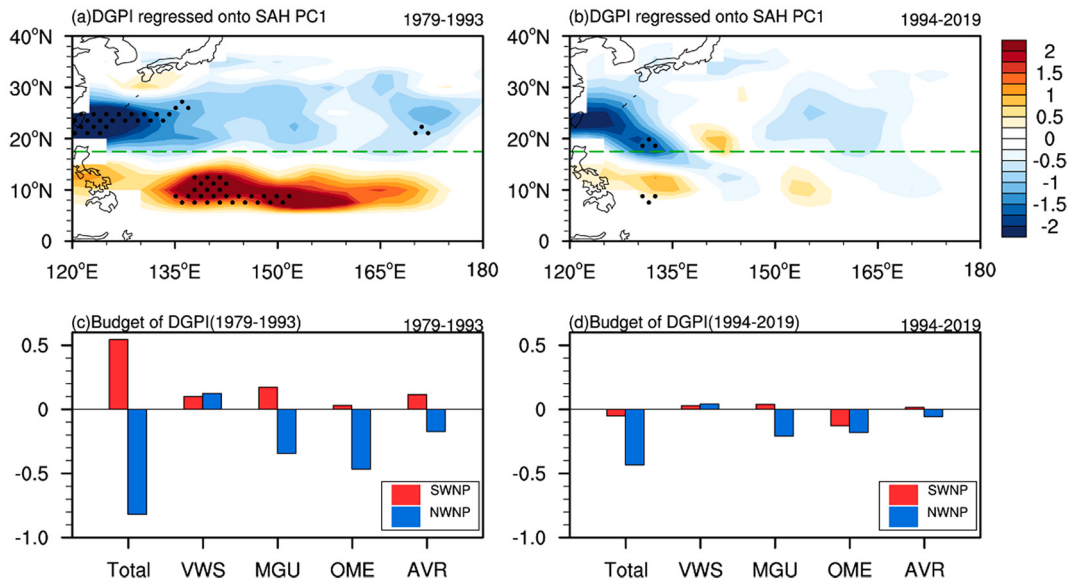


Fig. 5. Regressed DGPI against the SAH PC1 during July–September from (a) 1979–1993 and (b) 1994–2019. Budget analyses of the DGPI for the NWNP and SWNP during (c) 1979–1993 and (d) 1994–2019. Total, VWS, MGU, OME and AVR refer to the total DGPI, the role of vertical wind shear between 200 and 850-hPa, the role of the meridional gradient of zonal wind at 500-hPa, the role of 500-hPa vertical velocity, and the role of 850-hPa absolute vorticity, respectively. The values in (a) and (b) with black dots are significant at the 90% confidence level.

SWNP. Fig. 7 displays the regression pattern of 200-hPa and 850-hPa wind and SSTAs onto SAH PC1 for the two sub-periods. During the sub-period from 1979 to 1993, SSTA during strong SAH years shows an El Niño-like coupling pattern characterized by warm SSTAs in the equatorial eastern Pacific and the tropical northern Indian Ocean, with cold SSTAs in the equatorial western Pacific (Fig. 7a). A cyclonic circulation and equatorial westerly flow were generated to the northwest/west of the tropical Pacific heating source via a Gill-type response (Gill, 1980). Together with enhancement of anomalous westerly flow by the zonal SST gradient and Gill-type response, this circulation pattern enhanced cyclonic shear in the SWNP that consequently favored a cyclonic circulation over this region (Fig. 7a, c). In response to cyclonic circulation anomalies, there is anomalous ascending motion and increases in mid-level moisture over the SWNP, favoring more TCs over the SWNP sub-region (Fig. 6f). During 1994–2019, the weakening of warm SSTAs in the central-eastern Pacific and the disappearance of cold SSTAs in the western Pacific weakened the anomalous Walker circulation. These changes lead to weak equatorial westerly wind anomalies that thus only weakly affect TCGF over the SWNP basin (Figs. 6h, 7b, d).

When El Niño is in phase with the Pacific decadal oscillation (PDO) (e.g., a positive phase of the PDO), El Niño is strongly tied to anomalously warm Indian Ocean SSTAs, thus heating the troposphere and strengthening the SAH through a Gill-type response (Huang et al., 2011; Qu and Huang, 2012; Xue et al., 2018). Given that regressed SSTAs against SAH PC1 exhibited an El Niño-like coupling patterns during 1979–1993 with typical warm PDO features, we speculate that ENSO would also enhance the SAH. To further clarify this, we also compute correlations of the SAH with the Niño 3.4 index and North Indian Ocean (NIO, 15°N–25°N, 40°E–100°E) SSTAs during 1979–2019 (Fig. 8a). During 1979–2019, there are no significant simultaneous correlations between SAH PC1 and either the Niño 3.4 index or NIO SSTAs. However, SAH PC1 significantly correlates with the May–July Niño 3.4 index ($r = 0.57$) and with June–August NIO SSTAs up to 0.67 for 1979–1993. We further calculated the partial correlation coefficients of SAH PC1 with both the May–July Niño3.4 index ($r = 0.48$) and June–August NIO SSTAs ($r = 0.61$). After removing the correlation between the Niño3.4 index and NIO SSTAs, the only correlation that remains significant is between SAH PC1 and June–August NIO SSTAs. Additionally, regression patterns of the wind, surface temperature and tropospheric thickness

against SAH PC1 also indicate the occurrence of a Gill-type response in the Indian Ocean basin, thus enhancing the SAH in 1979–1993 (figure not shown). This observational evidence suggests that late spring ENSO can indirectly affect SAH via summer SSTAs in the Indian Ocean. When Indian Ocean SSTAs anomalously warm, it can favor suppression of NWNP TCGF.

In contrast, during 1994–2019, the effect of the coupled El Niño-like SST pattern on the inter-annual variability of SAH appears to be reduced, given the weakening of the coupled El Niño-like SST pattern. Although the combined effect of the in phase relationship between PDO and ENSO may play a role, the timing of the PDO phase shift does not coincide with the weakening of the SST pattern. To some extent, other factors likely cause the regime shift in the inter-annual relationship between the SAH and WNP TCGF. We intend to investigate these in future research.

4.2. Role of inter-decadal change of EASM in SAH

Prior studies have suggested that the EAJS is closely associated with the SAH (Wei et al., 2017). Due to a barotropic response driven by increased precipitation in southeastern China, Kwon (2005) suggested that there has been an inter-decadal weakening of the EAJS since 1994. Inter-decadal changes in the EASM that began in the early 1990s have been widely documented (Ding et al., 2008, 2009; Wu et al., 2008). Consistent with inter-decadal changes in the EASM, a significant weakening of the EAJS and its associated north-south temperature gradient in the troposphere have been observed (Zhang and Zhou, 2015). During this time, there has also been a significant increase of summer precipitation in southeastern China (Wu et al., 2010). We hypothesize that inter-decadal changes of the SAH are mainly associated with the EAJS and associated summer rainfall over southern China.

Following Kwon (2005), we next use 200-hPa JAS-mean zonal wind during July–September for the region spanning 35°N–40°N, 90°E–130°E to represent the EAJS. Agreeing well with prior studies (Wei et al., 2017), we find an extreme high correlation between the EAJS and the SAH ($r = 0.94$) during the whole period from 1979 to 2019 (Fig. 8b), indicating concurrent changes between the EAJS and SAH. The correlation between SAH PC1 and summer precipitation in southern China (20°N–25°N, 110°E–120°E) during June–August is significant ($r =$

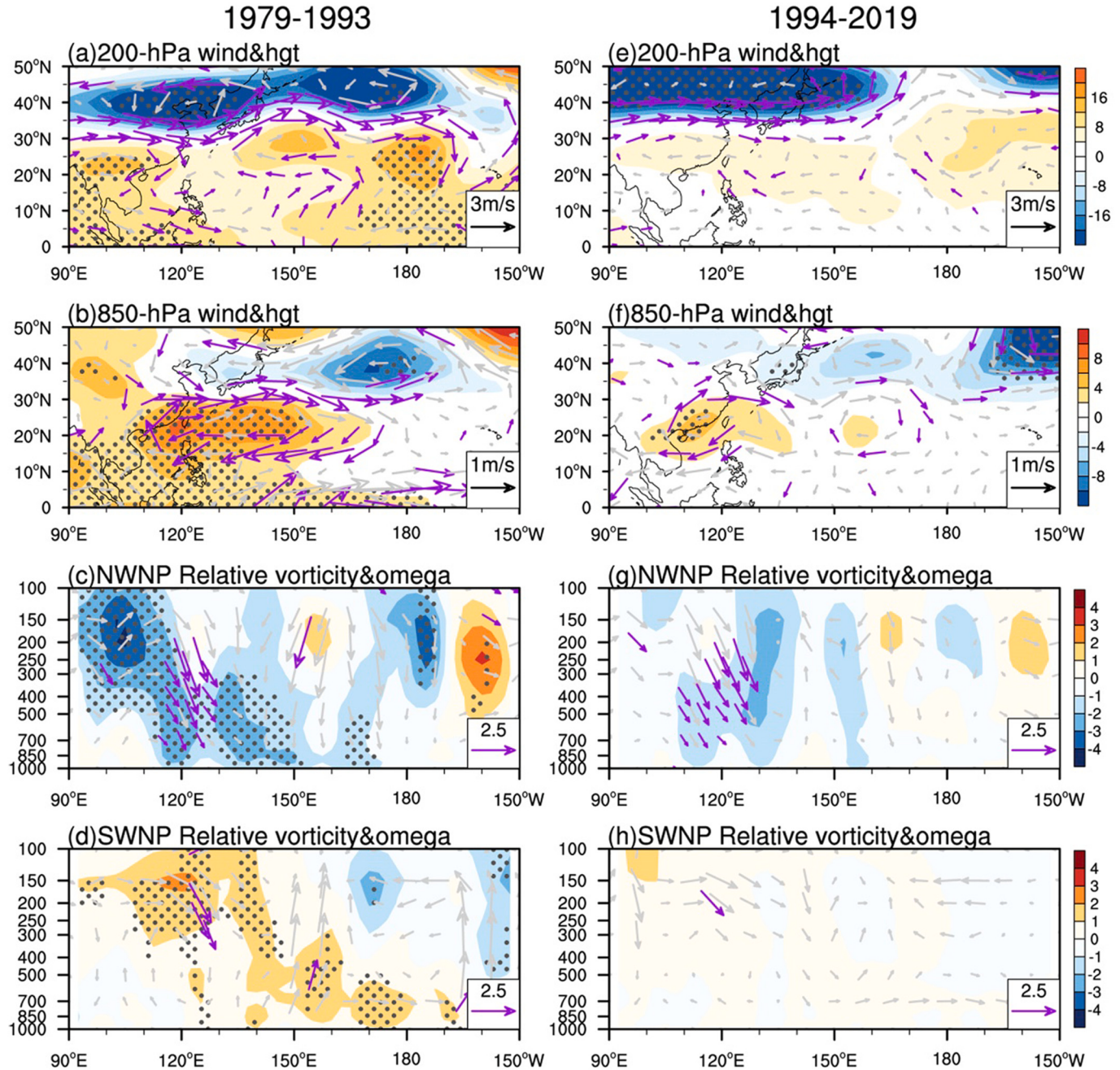


Fig. 6. Regressed horizontal wind (vector, units: m s^{-1}) and geopotential height (shading, units: gpm) against SAH PC1 at (a) 200-hPa and (b) 850-hPa and relative vorticity (shading, units: 10^{-6} s^{-1}) and mean vertical wind (vector, units: 10^{-4} m s^{-1}) in the (c) NWNP ($17.5\text{--}30^\circ\text{N}$) and (d) SWNP ($0\text{--}17.5^\circ\text{N}$) during July–September from 1979 to 1993. (e)–(h) as in (a)–(d) but for the period of 1994–2019. The values with purple vectors and gray dots are significant at the 90% confidence level. (For interpretation of the references to colour in this figure legend, the reader is referred to the web version of this article.)

–0.60), indicating that there is a significant negative correlation between southern China precipitation and SAH PC1 (Fig. 8b). We hypothesize that changes in the EASM since the early 1990s increased precipitation in southern China (Fig. 9a). As shown in Fig. 9b-d, the barotropic response of increased precipitation in southern China was accompanied by an increase in low-level cyclonic circulation and wind convergence, mid-level ascending motion and upper-level cyclonic circulation and wind divergence. These could be largely considered as a barotropic response to steady forcing from anomalous precipitation. The easterly winds to the north of the upper-level cyclone weaken the EAJS that had been located to the north of the upper-level cyclone (Fig. 9e).

Correspondingly, the SAH also weakens (Fig. 9d). Therefore, by changing the local circulation in East Asia, inter-decadal changes in the EASM likely caused the observed inter-decadal weakening of the east-central SAH. The causes of the inter-decadal shift in the EASM in the early 1990s are still debated and warrant further investigations.

4.3. Role of inter-decadal changes of the oceanic thermal state

Given the large impact of oceanic thermal inertia in maintaining atmospheric circulations (Shukla, 1998; Wang et al., 2005; Wang and Wang, 2021), we speculated that significant changes in the ocean

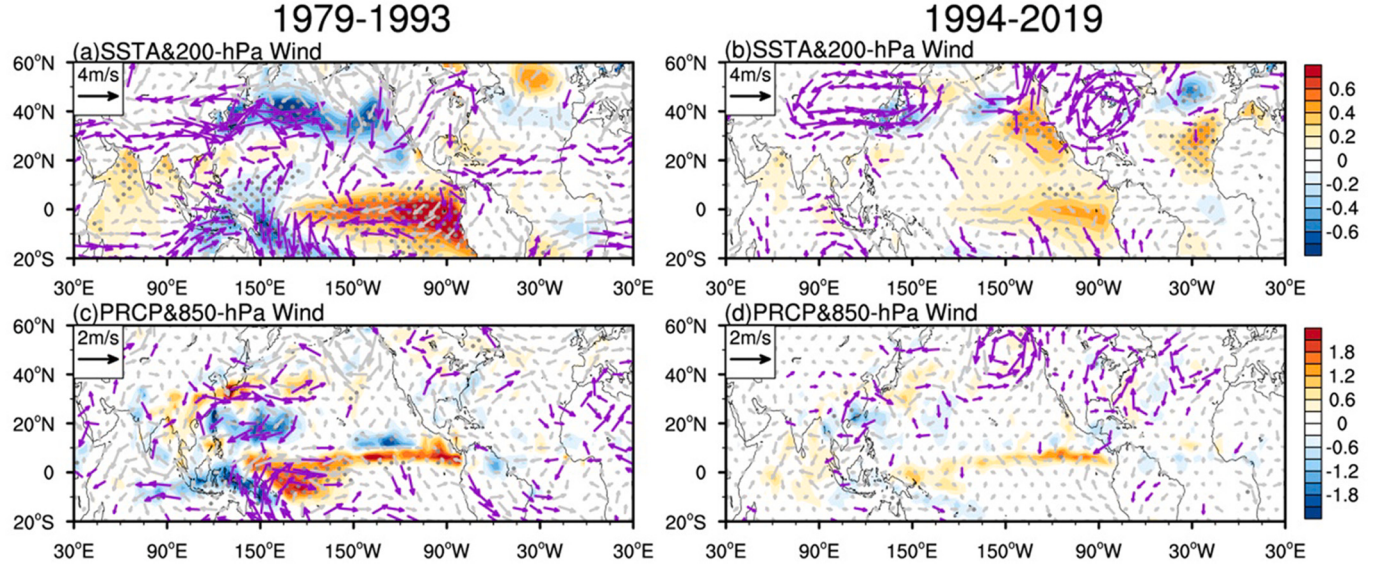


Fig. 7. As in Fig. 6, but for (a) SSTAs (shading, units: $^{\circ}\text{C}$) and 200-hPa wind (vector, units: m s^{-1}) from 1979 to 1993 and (b) precipitation (shading, units: mm day^{-1}) and 850-hPa wind (vector, units: m s^{-1}) from 1979 to 1993. (c)-(d) As in (a)-(b) but 1994–2019. Purple vectors and gray dots denote significance at the 90% confidence level. (For interpretation of the references to colour in this figure legend, the reader is referred to the web version of this article.)

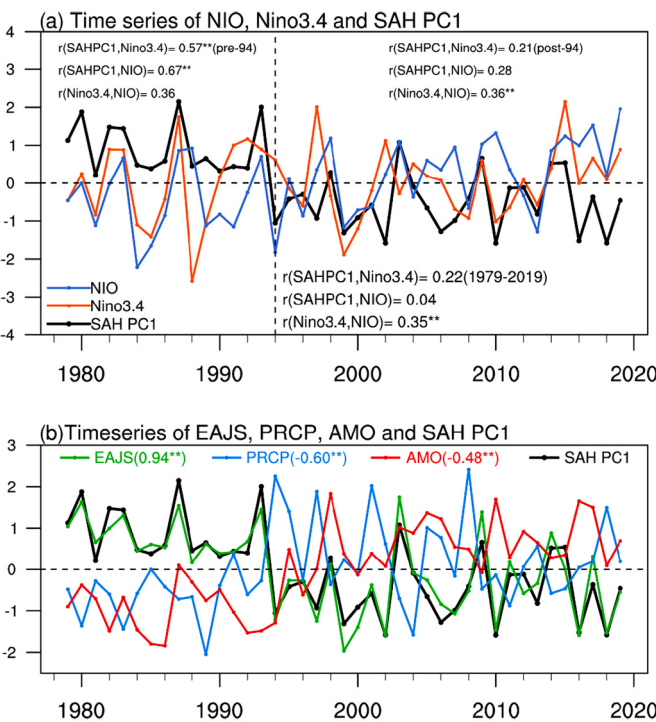


Fig. 8. (a) Standardized time series of SAH PC1, the Niño3.4 index and North Indian Ocean (NIO) [$15^{\circ}\text{N}-25^{\circ}\text{N}$, $40^{\circ}\text{E}-100^{\circ}\text{E}$], SSTAs from 1979 to 2019, Correlation coefficient (r) during the whole period of 1979–2019 (bottom of the panel) and the two sub-periods of 1979–1993 (top left of the panel) and 1994–2019 (top right of the panel) are shown. (b) Standardized time series of SAH PC1, the July–September East Asian Upper-Tropospheric Jet Stream (EAJS) that is defined by 200-hPa JAS-mean zonal wind from [$35^{\circ}\text{N}-40^{\circ}\text{N}$, $90^{\circ}\text{E}-130^{\circ}\text{E}$], JJA-mean precipitation averaged over [$20^{\circ}\text{N}-25^{\circ}\text{N}$, $110^{\circ}\text{E}-120^{\circ}\text{E}$], and the yearly mean AMO index from 1979 to 2019 along with their correlations with SAH PC1. The values that are significant at a 90% confidence level are denoted with the symbol ***.

thermal state that occurred in the mid-1990s (Fig. 9f) may play an important role in shaping the regime shift of the SAH and its association with TCF over WNP basin. As shown in Fig. 9f, there is an apparent phase shift of the AMO in the early to mid-1990s from its cool phase to its warm phase. Here, we focus on the role of the AMO phase shift in the interdecadal variability of the SAH.

During 1979–2019, the correlation between the AMO index and SAH PC1 is -0.48 , significant at a 99% confidence level using effective degrees of freedom. Regressed 200-hPa wind and eddy geopotential height during June–August against the AMO index show cyclonic and anticyclonic wave trains excited by the Atlantic SST anomaly (Fig. 10a). The eddy geopotential height refers to the departure of geopotential height from the zonal mean following Gao et al. (2021). Positive 200-hPa eddy geopotential height anomalies were located in the northwest Atlantic, central Europe and southwest Lake Baikal, while negative anomalies were located in the eastern-central Atlantic and western Asia. These results are consistent with prior studies of Atlantic SST anomalies affecting subtropical jet streams (Zhou et al., 2019; Sun et al., 2020; Gao et al., 2021). The wind and eddy geopotential height during July–September also show a similar wave train structure, with an anomalous anticyclone remaining over the Baikal region (Fig. 10b). Therefore, since the early to mid-1990s, the anomalous warming of the Atlantic Ocean associated with the AMO phase shift, has excited an eastward propagating Rossby wave over Eurasia, resulting in an anomalous anticyclone at 200-hPa over the Lake Baikal region, where easterly winds at the base of the anomalous anticyclone directly weakened the EAJS and SAH. In addition, the AMO phase shift also affects changes in the Pacific oceanic thermal state (McGregor et al., 2014; Kucharski et al., 2016; Sun et al., 2017). As shown by Fig. 9f and Fig. 10c-d, there has been a large and significant warming in the western tropical Pacific since 1994, while there has not been a significant change in SSTAs in the tropical central-eastern Pacific. The change of SSTAs in the tropical Pacific weakens zonal SST gradient in an El Niño event (Fig. 7a), leading to a weakening of the low-level anomalous westerly winds that enhanced the SWNP TCGF as mentioned in Fig. 7c (McGregor et al., 2014). In summary, changes of both the local large-scale circulation and oceanic thermal state cause an interdecadal weakening of the SAH and the reduction of the SAH-TC relationship during recent decades.

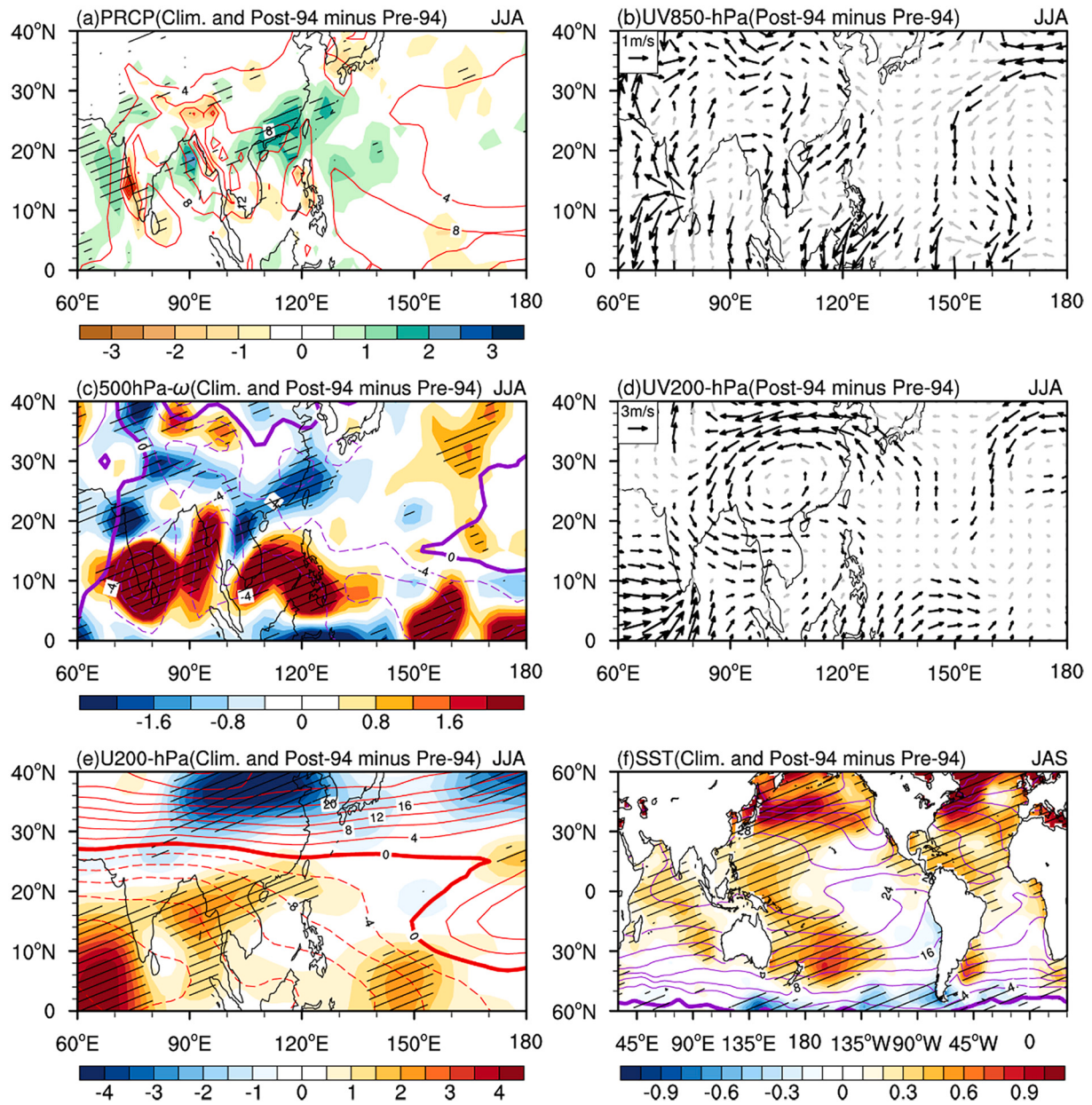


Fig. 9. Climatological mean during 1979–2019 (contours) and climatological mean during 1994–2019 minus climatological mean during 1979–1993 (shaded) of (a) JJA-mean precipitation (units: mm day^{-1}), (b) JJA-mean wind at 850-hPa (units: m s^{-1}), (c) JJA-mean vertical velocity at 500-hPa (units: $10^{-2} \text{ Pa s}^{-1}$), (d) JJA-mean wind at 200-hPa (units: m s^{-1}), (e) JJA-mean zonal wind (units: m s^{-1}) and (f) JAS-mean SST (units: $^{\circ}\text{C}$); The values with slashes in (a, c, e, f) and black vectors in (b, d) are significant at the 90% confidence level.

5. Summary and discussion

Studies have emphasized the importance of large-scale circulation systems in modulating WNP TC activity (Briegel and Frank, 1997; Wu et al., 2015; Wang and Wang, 2019, 2021; Wu et al., 2022), while inter-annual changes in the SAH and how those affect WNP TCs on inter-decadal time scales have been less studied. This study suggests that the relationship between the first SAH leading mode and the meridional TC distribution has experienced a significant climate regime shift. These changes are likely due to inter-decadal changes of the first SAH leading mode with a stronger SAH during 1979–1993 and a weakened SAH during 1994–2019.

During the whole period from 1979 to 2019 and both sub-periods, there are no significant associations between WNP TCGF and SAH PC1. However, during 1979–1993, when the SAH is stronger, we find a

meridional dipole pattern of WNP TCGF with suppressed TCGF over the northern WNP (NWNP) and enhanced TCGF over the southern WNP (SWNP) in response to inter-annual changes of the SAH. The NWNP TCGF has a significant negative correlation with the SAH ($r = -0.69$), while the SWNP TCGF has a significant positive correlation with the SAH ($r = 0.78$). This north-south seesaw pattern in TCGF has disappeared from 1994 to 2019. Additional composite analysis of the distribution of TCs confirms this result. Changes in large-scale environmental parameters during 1979–1993 can explain the inter-decadal modulation of the meridional variation of WNP TC generation by the SAH. The decrease (increase) of TCGF in the NWNP (SWNP) is consistent with large-scale environmental conditions of descending (ascending) motion, negative (positive) low-level vorticity, and suppressed (enhanced) moisture during 1979–1993. In contrast, changes in large-scale factors related to inter-annual SAH variability during

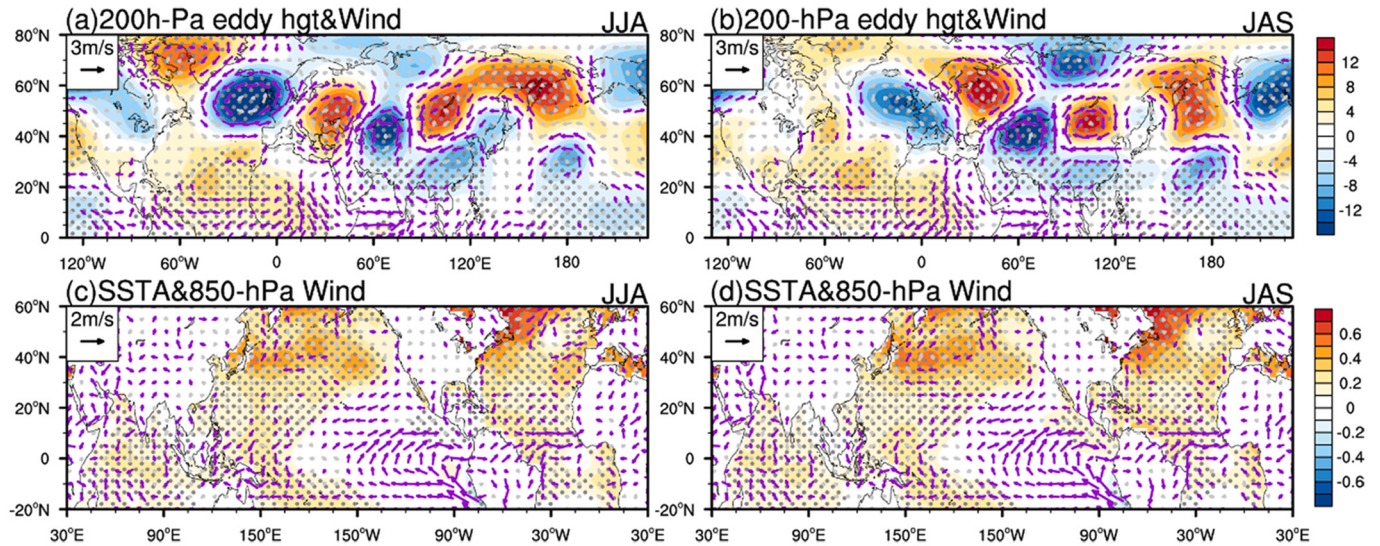


Fig. 10. (a) Regressed 200 hPa wind (vector, units: m s^{-1}) and eddy geopotential height (shading, units: gpm) anomalies that refers to the departure of geopotential height from the zonal mean, (c) Regressed 850 hPa wind (vector, units: m s^{-1}) and SST (shading, units: $^{\circ}\text{C}$) anomalies against the AMO index during June–August from 1979 to 2019. (b), (d) as in (a), (c) but for the month of July–September. The values with black vectors and gray dots are significant at the 90% confidence level.

1994–2019 are relatively weak. A budget analysis of the DGPI reveals that different large-scale factors influenced TCGF in the two sub-regions, with the NWNP dominated by mid-level vertical motion and the SWNP dominated by low-level absolute vorticity.

Inter-decadal changes in large-scale factors are associated with inter-decadal changes of the SAH and EAJS. During 1979–1993, when the SAH shifted southward and was relatively strong, the SAH and EAJS concurrently produced low-level negative vorticity, leading to the maintenance of a strong anticyclonic circulation at low levels that suppressed TC formation over the NWNP. Meanwhile, via a Gill-type response, a cyclonic circulation occurs in the SWNP basin, with anomalous equatorial westerly winds driven by anomalously warm SSTAs in the eastern central tropical Pacific as well as easterly winds on the southern end of the anomalous anticyclone over the NWNP. Both of these wind patterns are forced by cyclonic shear, favoring TC formation in the SWNP. Moreover, the El Niño-like SST coupling pattern also can enhance the SAH via a Gill-type response in the Indian Ocean, thereby suppressing NWNP TCGF. We also show that the inter-decadal weakening of the leading mode of the SAH occurred in the early to mid-1990s, weakening the relationship between the SAH and TCGF.

These observed inter-decadal changes in the SAH and EAJS are possibly due to inter-decadal changes of the EASM and AMO that occurred in the early to mid-1990s. The inter-decadal variability of the EASM in the early 1990s increased precipitation over southern China. Increased low-level convergence, mid-level ascending motion and upper-level divergence occurred over southern China due to the barotropic response to increased precipitation. This barotropic response also reduced westerly winds to the north of the anomalous cyclone, causing an interdecadal weakening of the SAH and EAJS. Meanwhile, the AMO phase shift from its cool to its warm phase significantly increased North Atlantic SST anomalies. The positive SST anomaly in the northwest Atlantic induced an eastward propagating Rossby wave train in the upper troposphere (Zhou et al., 2019; Sun et al., 2020; Gao et al., 2021), which crosses Eurasia and eventually formed an anticyclonic circulation in the Baikal region. The easterly winds to the south of the anticyclonic circulation also weakened the westerly winds to the north of the EAJS and SAH. Additionally, the western Pacific SST anomaly associated with the AMO phase shift decreases the zonal SST gradient, leading to the weakening of the low-level anomalous westerly winds and thus enhancing the SWNP TCGF. Wang et al. (2017) suggested that the

enhanced Atlantic-Pacific capacitance effect and the weakened Pacific-Indian Ocean capacitance effect since the early-1990s is consistent with the AMO phase shift. To some degree, the phase shift of the AMO potentially plays a considerable role in causing the interdecadal weakening of the SAH and EAJS and the disappearance of the SAH-TC relationship. We intend to investigate these relationships in more detail in future work.

CRediT authorship contribution statement

Yuqi Zang: Methodology, Software, Visualization, Writing – original draft. **Haikun Zhao:** Conceptualization, Supervision, Investigation, Writing – original draft, Writing – review & editing. **Philip J. Klotzbach:** Writing – review & editing. **Chao Wang:** Writing – review & editing. **Jian Cao:** Writing – review & editing.

Declaration of Competing Interest

The authors declare no competing financial interests. If you have any questions regarding this manuscript, please contact me at zhk2004y@gmail.com or haikunzhao@nuist.edu.cn. Thank you very much for your consideration.

Data availability

Data will be made available on request.

Acknowledgements

This research was jointly supported by the National Natural Science Foundation of China (Grant 42192551, 41922033, 41730961) and the Six Talent Peaks project in Jiangsu Province (JY-100). P. Klotzbach would like to acknowledge a grant from the G. Unger Vetlesen Foundation. We acknowledge the High Performance Computing Center of Nanjing University of Information Science and Technology for their support of this work.

References

- Adler, R.F., et al., 2018. The Global Precipitation Climatology Project (GPCP) monthly analysis (new version 2.3) and a review of 2017 global precipitation. *Atmos.* 9 <https://doi.org/10.3390/atmos9040138>.
- Bretherton, C.S., Widmann, M., Dymnikov, V.P., Wallace, J.M., Blade, I., 1999. The effective number of spatial degrees of freedom of a time-varying field. *J. Clim.* 12, 1990–2009. [https://doi.org/10.1175/1520-0442\(1999\)012%3C1990:TENOSD%3E2.0.CO;2](https://doi.org/10.1175/1520-0442(1999)012%3C1990:TENOSD%3E2.0.CO;2).
- Briegel, L.M., Frank, W.M., 1997. Large-scale influences on tropical cyclogenesis in the Western North Pacific. *Mon. Weather Rev.* 125, 1397–1413. [https://doi.org/10.1175/1520-0493\(1997\)125<1397:LSIOTC>2.0.CO;2](https://doi.org/10.1175/1520-0493(1997)125<1397:LSIOTC>2.0.CO;2).
- Camargo, S.J., Sobel, A.H., 2005. Western North Pacific tropical cyclone intensity and ENSO. *J. Clim.* 18, 2996–3006. https://doi.org/10.1175/jcli3_457.1.
- Cao, X., et al., 2016. Intensified impact of northern tropical Atlantic SST on tropical cyclogenesis frequency over the western North Pacific after the late 1980s. *Adv. Atmos. Sci.* 33, 919–930. <https://doi.org/10.1007/s00376-016-5206-z>.
- Chan, J.C.L., 2005. Interannual and interdecadal variations of tropical cyclone activity over the western North Pacific. *Meteorog. Atmos. Phys.* 89, 143–152. <https://doi.org/10.1007/s00703-005-0126-y>.
- Chen, T.-C., et al., 2004. Role of the Monsoon Gyre in the interannual variation of tropical cyclone formation over the Western North Pacific. *Wea. Forecast.* 19, 776–785. [https://doi.org/10.1175/1520-0434\(2004\)019<0776:ROTMDI>2.0.CO;2](https://doi.org/10.1175/1520-0434(2004)019<0776:ROTMDI>2.0.CO;2).
- Chen, S., et al., 2021a. Decadal modulation of transbasin variability on extended boreal summer tropical cyclone activity in the tropical North Pacific and Atlantic Basins. *J. Clim.* 34, 7149–7166. <https://doi.org/10.1175/JCLI-D-20-0249.1>.
- Chen, S., et al., 2021b. Modulation of North Pacific and North Atlantic tropical cyclones by tropical transbasin variability and ENSO during May–October. *J. Clim.* 34, 2127–2144. <https://doi.org/10.1175/JCLI-D-19-0866.1>.
- Chu, J.-H., Sampson, C.R., Levine, A.S., Fukada, E., 2002. The joint typhoon warning center tropical cyclone best-tracks, 1945–2000. In: Naval Research Lab Rep. NRL/MR/7540-02-16. http://www.usno.navy.mil/NOOC/nmc-ph/RSS/jtwc/best_track_s/TC_bt_report.html.
- Ding, Y., et al., 2008. Inter-decadal variation of the summer precipitation in East China and its association with decreasing Asian summer monsoon. Part I: Observed evidences. *Int. J. Climatol.* 28, 1139–1161. <https://doi.org/10.1002/joc.1615>.
- Ding, Y., et al., 2009. Inter-decadal variation of the summer precipitation in China and its association with decreasing Asian summer monsoon Part II: possible causes. *Int. J. Climatol.* 29, 1926–1944. <https://doi.org/10.1002/joc.1759>.
- Emanuel, K.A., Nolan, D.S., 2004. Tropical cyclone activity and global climate. In: Proc. of 26th Conf. on Hurricanes and Tropical Meteorology. American Meteorological Society, Miami, FL, pp. 240–241.
- Flohn, H., 1957. Large-scale Aspects of the Summer Monsoon in South and East Asia. *J. Meteor. Soc. Japan Ser. II* 35A, 180–186. https://doi.org/10.2151/jmsj1923.35A.0_180.
- Gao, K., Duan, A., Chen, D., 2021. Interdecadal summer warming of the Tibetan Plateau potentially regulated by a sea surface temperature anomaly in the Labrador Sea. *Int. J. Climatol.* 41 (Suppl. 1), E2633–E2643. <https://doi.org/10.1002/joc.6871>.
- Geng, X., et al., 2020. Modulation of the relationship between ENSO and its combination mode by the Atlantic multidecadal oscillation. *J. Clim.* 33, 4679–4695. <https://doi.org/10.1175/jcli-d-19-0740.1>.
- Gill, A., 1980. Some simple solutions for heat-induced tropical circulation. *Quart. J. Roy. Meteor. Soc.* 106, 447–462. <https://doi.org/10.1002/qj.49110644905>.
- Guo, Y.-P., Tan, Z.-M., 2018. Westward migration of tropical cyclone rapid-intensification over the Northwestern Pacific during short duration El Niño. *Nat. Commun.* 9, 1507. <https://doi.org/10.1038/s41467-018-03945-y>.
- Guo, Y.-P., Tan, Z.-M., 2021. Influence of different ENSO types on tropical cyclone rapid intensification over the western North Pacific. *J. Geophys. Res. Atmos.* 126, e2020JD033059. <https://doi.org/10.1029/2020JD033059>.
- Ha, Y., Zhong, Z., Yang, X., Sun, Y., 2015. Contribution of East Indian Ocean SSTAs to Western North Pacific tropical cyclone activity under El Niño/La Niña conditions. *Int. J. Climatol.* 35, 506–519. <https://doi.org/10.1002/joc.3997>.
- Hersbach, H., et al., 2020. The ERA5 global reanalysis. *Quart. J. Roy. Meteor. Soc.* 146, 1999–2049. <https://doi.org/10.1002/qj.3803>.
- Hoskins, B.J., Rodwell, M.J., 1995. A model of the Asian summer monsoon. Part I: The global scale. *J. Atmos. Sci.* 52, 1329–1340. [https://doi.org/10.1175/1520-0469\(1995\)052<1329:AMOTAS>2.0.CO;2](https://doi.org/10.1175/1520-0469(1995)052<1329:AMOTAS>2.0.CO;2).
- Huang, G., et al., 2011. The impact of the tropical Indian Ocean on South Asian High in boreal summer. *Adv. Atmos. Sci.* 28, 421–432. <https://doi.org/10.1007/s00376-010-9224-y>.
- Huang, B., et al., 2017. Extended reconstructed sea surface temperature, version 5 (ERSSTv5): upgrades, validations, and intercomparisons. *J. Clim.* 30, 8179–8205. <https://doi.org/10.1175/jcli-d-16-0836.1>.
- Huo, L., et al., 2015. The role of tropical Atlantic SST anomalies in modulating western North Pacific tropical cyclone genesis. *Geophys. Res. Lett.* 42, 2378–2384. <https://doi.org/10.1002/2015GL063184>.
- Jiang, X., et al., 2011. Interannual and interdecadal variations of the South Asian and western Pacific subtropical highs and their relationships with Asian-Pacific summer climate. *Meteorog. Atmos. Phys.* 113, 171–180. <https://doi.org/10.1007/s00703-011-0146-8>.
- Kanamitsu, M., et al., 2002. NCEP–DOE AMIP-II reanalysis (R-2). *Bull. Amer. Meteor. Soc.* 83, 1631–1644. <https://doi.org/10.1175/bams-83-11-1631>.
- Kobayashi, S., et al., 2015. The JRA-55 reanalysis: general specifications and basic characteristics. *J. Meteor. Soc. Japan Ser. II* 93, 5–48. <https://doi.org/10.2151/jmsj.2015-001>.
- Krishnamurti, T.N., et al., 1973. Tibetan high and upper tropospheric tropical circulations during northern summer. *Bull. Am. Meteorol. Soc.* 54, 1234–1250. <https://doi.org/10.1175/1520-0477-54.12.1234>.
- Kucharski, F., Parvin, A., Rodriguez-Fonseca, B., Farneti, R., Martin-Rey, M., Polo, I., Mohino, E., Losada, T., Mechoso, C.R., 2016. The teleconnection of the tropical atlantic to indo-pacific sea surface temperatures on inter-annual to centennial time scales: a review of recent findings. *Atmos.* 7, 29. <https://doi.org/10.3390/atmos7020029>.
- Kwon, M., 2005. Decadal change in relationship between east Asian and WNP summer monsoons. *Geophys. Res. Lett.* 32 <https://doi.org/10.1029/2005gl023026>.
- Liebmann, B., Smith, C.A., 1996. Description of a complete (interpolated) outgoing longwave radiation dataset. *Bull. Amer. Meteor. Soc.* 77 (6), 1275–1277. <http://www.jstor.org/stable/26233278>.
- Liu, K.S., Chan, J.C.L., 2013. Inactive period of Western North Pacific tropical cyclone activity in 1998–2011. *J. Clim.* 26, 2614–2630. <https://doi.org/10.1175/JCLI-D-12-00053.1>.
- Liu, B., et al., 2013. Genesis of the South Asian high and its impact on the Asian Summer Monsoon onset. *J. Clim.* 26, 2976–2991. <https://doi.org/10.1175/JCLI-D-12-00286.1>.
- Liu, H.-Y., Gu, J.-F., Wang, Y., Xu, J., 2022. Contributions of anomalous large-scale circulations to the absence of tropical cyclones over the western North Pacific in July 2020. *Geophys. Res. Lett.* 49, e2021GL096652. <https://doi.org/10.1029/2021GL096652>.
- Lu, Y., Zhao, H., Zhao, D., et al., 2021. Spatial-temporal characteristic of tropical cyclone disasters in China during 1984–2017. *Acta Oceanol. Sin. (in chineses)* 43 (6), 1–17.
- Mason, R.B., Anderson, C.E., 1963. The development and decay of the 100-mb summertime anticyclone over southern Asia. *Mon. Weather Rev.* 91, 3–12. [https://doi.org/10.1175/1520-0493\(1963\)091<0003:Tdadot>2.3.Co;2](https://doi.org/10.1175/1520-0493(1963)091<0003:Tdadot>2.3.Co;2).
- McGregor, S., Timmermann, A., Stuecker, M., et al., 2014. Recent walker circulation strengthening and Pacific cooling amplified by Atlantic warming. *Nat. Clim. Chang.* 4, 888–892. <https://doi.org/10.1038/nclimate2330>.
- Murakami, H., Wang, B., 2022. Patterns and frequency of projected future tropical cyclone genesis are governed by dynamic effects. *Commun. Earth Environ.* 3, 77. <https://doi.org/10.1038/s43247-022-00410-z>.
- Ning, L., et al., 2017. How does the South Asian High influence extreme precipitation over eastern China? *J. Geophys. Res.-Atmos.* 122, 4281–4298. <https://doi.org/10.1002/2016JD026075>.
- Nützel, M., et al., 2016. Movement, drivers and bimodality of the South Asian High. *Atmos. Chem. Phys.* 16, 14755–14774. <https://doi.org/10.5194/acp-16-14755-2016>.
- Patricola, C.M., et al., 2018. The influence of ENSO flavors on Western North Pacific tropical cyclone activity. *J. Clim.* 31, 5395–5416. <https://doi.org/10.1175/jcli-d-17-0678.1>.
- Peduzzi, P., et al., 2012. Global trends in tropical cyclone risk. *Nat. Clim. Chang.* 2, 289–294. <https://doi.org/10.1038/nclimate1410>.
- Peiquan, Z., et al., 2005. South Asian high and Asian-Pacific-American climate teleconnection. *Adv. Atmos. Sci.* 22, 915–923. <https://doi.org/10.1007/BF2918690>.
- Qu, X., Huang, G., 2012. An enhanced influence of tropical Indian Ocean on the South Asia high after the late 1970s. *J. Clim.* 25 (20), 6930–6941. <https://doi.org/10.1175/JCLI-D-11-00696.1>.
- Ren, X., et al., 2015. Characteristics and mechanisms of the subseasonal eastward extension of the South Asian High. *J. Clim.* 28, 6799–6822. <https://doi.org/10.1175/JCLI-D-14-00682.1>.
- Ritchie, E.A., Holland, G.J., 1999. Large-scale patterns associated with tropical cyclogenesis in the Western Pacific. *Mon. Weather Rev.* 127, 2027–2043. [https://doi.org/10.1175/1520-0493\(1999\)127<2027:LSPAWT>2.0.CO;2](https://doi.org/10.1175/1520-0493(1999)127<2027:LSPAWT>2.0.CO;2).
- Schreck III, C.J., Knapp, K.R., Kossin, J.P., 2014. The impact of best track discrepancies on global tropical cyclone climatologies using IBTrACS. *Mon. Weather Rev.* 142 (10), 3881–3899. <https://doi.org/10.1175/MWR-D-14-0002.1>.
- Shi, J., Qian, W., 2016. Connection between anomalous zonal activities of the South Asian high and Eurasian summer climate anomalies. *J. Clim.* 29, 8249–8267. <https://doi.org/10.1175/JCLI-D-15-0823.1>.
- Shukla, J., 1998. Predictability in the midst of chaos: a scientific basis for climate forecasting. *Science* 282, 728–731. <https://doi.org/10.1126/science.282.5389.728>.
- Sun, C., Kucharski, F., Li, J., et al., 2017. Western tropical Pacific multidecadal variability forced by the Atlantic multidecadal oscillation. *Nat. Commun.* 8, 15998. <https://doi.org/10.1038/ncomms15998>.
- Sun, J., Yang, K., Guo, W., Wang, Y., He, J., Lu, H., 2020. Why has the Inner Tibetan Plateau become wetter since the Mid-1990s? *J. Clim.* 33 (19), 8507–8522. <https://doi.org/10.1175/JCLI-D-19-0471.1>.
- Tao, S., Zhu, F., 1964. The 100 mb flow patterns in southern Asia in summer and its relation to the advance and retreat of the west pacific subtropical anticyclone over the far east. *Acta Meteorol. Sin. (in Chinese)* 34, 385–396. <https://doi.org/10.1167/qxb1964.039>.
- Trenberth, Kevin, National Center for Atmospheric Research Staff, 21 Jan 2020. The Climate Data Guide: Nino SST Indices (Nino 1+2, 3, 3.4, 4; ONI and TNI). Retrieved from. <https://climatedataguide.ucar.edu/climate-data/nino-sst-indices-nino-1-3-34-4-oni-and-tni>.
- Trenberth, Kevin, Zhang, Rong, National Center for Atmospheric Research Staff, 05 Jun 2021. The Climate Data Guide: Atlantic Multi-decadal Oscillation (AMO). Retrieved from. <https://climatedataguide.ucar.edu/climate-data/atlantic-multi-decadal-oscillation-amo>.
- Wang, B., 1992. The vertical structure and development of the ENSO anomaly mode during 1979–1989. *J. Atmos. Sci.* 49, 698–712. [https://doi.org/10.1175/1520-0469\(1992\)049<0698:Tvsado>2.0.Co;2](https://doi.org/10.1175/1520-0469(1992)049<0698:Tvsado>2.0.Co;2).

- Wang, B., Chan, J.C.L., 2002. How strong ENSO events affect tropical storm activity over the Western North Pacific? *J. Clim.* 15, 1643–1658. [https://doi.org/10.1175/1520-0442\(2002\)015<1643:Hseat>2.0.Co;2](https://doi.org/10.1175/1520-0442(2002)015<1643:Hseat>2.0.Co;2).
- Wang, B., Murakami, H., 2020. Dynamic genesis potential index for diagnosing present-day and future global tropical cyclone genesis. *Environ. Res. Lett.* 15 <https://doi.org/10.1088/1748-9326/abb001>.
- Wang, C., Wang, B., 2019. Tropical cyclone predictability shaped by western Pacific subtropical high: integration of trans-basin sea surface temperature effects. *Clim. Dyn.* 53, 2697–2714. <https://doi.org/10.1007/s00382-019-04651-1>.
- Wang, C., Wang, B., 2021. Impacts of the South Asian high on tropical cyclone genesis in the South China Sea. *Clim. Dyn.* 56, 2279–2288. <https://doi.org/10.1007/s00382-020-05586-8>.
- Wang, C., Wu, L., 2016. Interannual shift of the tropical Upper-Tropospheric trough and its influence on tropical cyclone formation over the Western North Pacific. *J. Clim.* 29, 4203–4211. <https://doi.org/10.1175/JCLI-D-15-0653.1>.
- Wang, C., Wu, L., 2018. Future changes of the monsoon trough: sensitivity to sea surface temperature gradient and implications for tropical cyclone activity. *Earth's Futur.* <https://doi.org/10.1029/2018EF000858>.
- Wang, B., et al., 2000. Pacific–East Asian teleconnection: How does ENSO affect East Asian Climate? *J. Clim.* 13, 1517–1536. [https://doi.org/10.1175/1520-0442\(2000\)013<1517:Peathd>2.0.Co;2](https://doi.org/10.1175/1520-0442(2000)013<1517:Peathd>2.0.Co;2).
- Wang, B., Ding, Q., Fu, X., Kang, I.-S., Jin, K., Shukla, J., Doblas-Reyes, F., 2005. Fundamental challenge in simulation and prediction of summer monsoon rainfall. *Geophys. Res. Lett.* 32, L15711. <https://doi.org/10.1029/2005GL022734>.
- Wang, B., et al., 2013. Subtropical High predictability establishes a promising way for monsoon and tropical storm predictions. *Proc. Natl. Acad. Sci.* 110, 2718–2722. <https://doi.org/10.1073/pnas.1214626110>.
- Wang, L., et al., 2017. Enhanced biennial variability in the Pacific due to Atlantic capacitor effect. *Nat. Commun.* 8, 14887. <https://doi.org/10.1038/ncomms14887>.
- Wang, C., Wang, B., Wu, L., 2019. Abrupt breakdown of the predictability of early season typhoon frequency at the beginning of the twenty-first century. *Clim. Dyn.* 52, 3809–3822. <https://doi.org/10.1007/s00382-018-4350-9>.
- Wei, W., Zhang, R., Wen, M., Yang, S., 2017. Relationship between the Asian Westerly Jet stream and summer rainfall over Central Asia and North China: roles of the Indian Monsoon and the South Asian High. *J. Clim.* 30 (2), 537–552. <https://doi.org/10.1175/JCLI-D-15-0814.1>.
- Wei, W., Zhang, R., Wen, M., Yang, S., Li, W., 2019. Dynamic effect of the South Asian high on the interannual zonal extension of the western North Pacific subtropical high. *Int. J. Clim.* 39, 5367–5379. <https://doi.org/10.1002/jo.c.6160>.
- Wu, L., Wang, C., 2015. Has the Western Pacific subtropical high extended Westward since the late 1970s? *J. Clim.* 28, 5406–5413. <https://doi.org/10.1175/JCLI-D-14-00618.1>.
- Wu, B., et al., 2008. Distinct modes of the East Asian Summer Monsoon. *J. Clim.* 21, 1122–1138. <https://doi.org/10.1175/2007JCLI1592.1>.
- Wu, R., et al., 2010. An interdecadal change in Southern China Summer rainfall around 1992/93. *J. Clim.* 23, 2389–2403. <https://doi.org/10.1175/2009JCLI3336.1>.
- Wu, L., et al., 2012. Possible linkage between the Monsoon trough variability and the tropical cyclone activity over the Western North Pacific. *Mon. Weather Rev.* 140, 140–150. <https://doi.org/10.1175/MWR-D-11-00078.1>.
- Wu, L., et al., 2015. Westward shift of western North Pacific tropical cyclogenesis. *Geophys. Res. Lett.* 42, 1537–1542. <https://doi.org/10.1002/2015GL063450>.
- Wu, L., et al., 2017. Insensitivity of the Summer South Asian high intensity to a warming Tibetan Plateau in modern reanalysis datasets. *J. Clim.* 30, 3009–3024. <https://doi.org/10.1175/jcli-d-16-0359.1>.
- Wu, L., et al., 2022. Understanding of the effect of climate change on tropical cyclone intensity: a review. *Adv. Atmos. Sci.* 39, 205–221. <https://doi.org/10.1007/s00376-021-1026-x>.
- Xiao, D., Li, J., 2007. Spatial and temporal characteristics of the decadal abrupt changes of global atmosphere-ocean system in the 1970s. *J. Geophys. Res.* 112, D24S22. <https://doi.org/10.1029/2007JD008956>.
- Xiao, D., et al., 2012. Four-dimensional structures and physical process of the decadal abrupt changes of the northern extratropical ocean–atmosphere system in the 1980s. *Int. J. Climatol.* 32, 983–994. <https://doi.org/10.1002/joc.2326>.
- Xue, X., et al., 2015. Modulation of the connection between boreal winter ENSO and the South Asian high in the following summer by the stratospheric quasi-biennial oscillation. *J. Geophys. Res.-Atmos.* 120, 7393–7411. <https://doi.org/10.1002/2015JD023260>.
- Xue, X., et al., 2017. The climatology and interannual variability of the South Asia high and its relationship with ENSO in CMIP5 models. *Clim. Dyn.* 48, 3507–3528. <https://doi.org/10.1007/s00382-016-3281-6>.
- Xue, X., et al., 2018. PDO modulation of the ENSO impact on the summer South Asian high. *Clim. Dyn.* 50, 1393–1411. <https://doi.org/10.1007/s00382-017-3692-z>.
- Yang, S., Li, T., 2016. Zonal shift of the South Asian High on the sub-seasonal time-scale and its relation to the summer rainfall anomaly in China. *Quart. J. Roy. Meteor. Soc.* 142, 2324–2335. <https://doi.org/10.1002/qj.2826>.
- Yu, J., et al., 2016. Effects of tropical North Atlantic SST on tropical cyclone genesis in the western North Pacific. *Clim. Dyn.* 46, 865–877. <https://doi.org/10.1007/s00382-015-2618-x>.
- Zhan, R., et al., 2011. Contributions of ENSO and East Indian Ocean SSTAs to the interannual variability of Northwest Pacific tropical cyclone frequency. *J. Clim.* 24, 509–521. <https://doi.org/10.1175/2010JCLI3808.1>.
- Zhang, L., Zhou, T., 2015. Decadal change of East Asian summer tropospheric temperature meridional gradient around the early 1990s. *Sci. China Earth Sci.* 58, 1609–1622. <https://doi.org/10.1007/s11430-015-5117-3>.
- Zhang, Q., et al., 2002. The bimodality of the 100-hPa South Asia high and its relationship to the climate anomaly over East Asia in summer. *J. Meteor. Soc. Japan Ser. II* 80, 733–744. <https://doi.org/10.2151/jmsj.80.733>.
- Zhang, Q., et al., 2009. Tropical cyclone damages in China 1983–2006. *Bull. Amer. Meteor. Soc.* 90, 489–496. <https://doi.org/10.1175/2008bams2631.1>.
- Zhang, W., et al., 2016. The Pacific meridional mode and the occurrence of tropical cyclones in the Western North Pacific. *J. Clim.* 29, 381–398. <https://doi.org/10.1175/JCLI-D-15-0282.1>.
- Zhang, D., et al., 2021. Is there Interdecadal variation in the South Asian High? *J. Clim.* 34, 8089–8103. <https://doi.org/10.1175/jcli-d-21-0059.1>.
- Zhao, H., Raga, G.B., 2014. The influence of large-scale circulations on the extremely inactive tropical cyclone activity in 2010 over the western North Pacific. *Atmósfera* 27, 353–365. [https://doi.org/10.1016/S0187-6236\(14\)70034-7](https://doi.org/10.1016/S0187-6236(14)70034-7).
- Zhao, H., Wang, C., 2016. Interdecadal modulation on the relationship between ENSO and typhoon activity during the late season in the western North Pacific. *Clim. Dyn.* 47, 315–328. <https://doi.org/10.1007/s00382-015-2837-1>.
- Zhao, H., Wang, C., 2019. On the relationship between ENSO and tropical cyclones in the western North Pacific during the boreal summer. *Clim. Dyn.* 52, 275–288. <https://doi.org/10.1007/s00382-018-4136-0>.
- Zhao, P., et al., 2009. Remotely modulated tropical-North Pacific Ocean–atmosphere interactions by the South Asian high. *Atmos. Res.* 94, 45–60. <https://doi.org/10.1016/j.atmosres.2009.01.018>.
- Zhao, H., Wu, L., Zhou, W., 2011. Interannual changes of tropical cyclone intensity in the Western North Pacific. *J. Meteor. Soc. Japan Ser. II* 89 (3), 243–253. <https://doi.org/10.2151/jmsj.2011-305>.
- Zhao, H., Klotzbach, P.J., Chen, S., 2020. Dominant influence of ENSO-like and global sea surface temperature patterns on changes in prevailing boreal summer tropical cyclone tracks over the Western North Pacific. *J. Clim.* 33 (22), 9551–9565. <https://doi.org/10.1175/JCLI-D-19-0774.1>.
- Zhou, N., et al., 2009. Bimodality of the South Asia High simulated by coupled models. *Adv. Atmos. Sci.* 26, 1226. <https://doi.org/10.1007/s00376-009-7219-3>.
- Zhou, C., Zhao, P., Chen, J., 2019. The interdecadal change of summer water vapor over the Tibetan Plateau and associated mechanisms. *J. Clim.* 32 (13), 4103–4119. <https://doi.org/10.1175/JCLI-D-18-0364.1>.